A&A 436, 101–115 (2005)
DOI: 10.1051/0004-6361:20052867

Astronomy & Astrophysics

Westerbork H I observations of high-velocity clouds near M 31 and M 33

T. Westmeier[1,2], R. Braun[2], and D. Thilker[3]

[1] Radioastronomisches Institut der Universität Bonn, Auf dem Hügel 71, 53121 Bonn, Germany
e-mail: twestmei@astro.uni-bonn.de
[2] ASTRON, PO Box 2, 7990 AA Dwingeloo, The Netherlands
[3] Center for Astrophysical Sciences, Johns Hopkins University, 3400 North Charles Street, Baltimore, MD 21218, USA

Received 11 February 2005 / Accepted 28 February 2005

Abstract. We have undertaken high-resolution follow-up of a sample of high velocity H I clouds apparently associated with M 31. Our sample was chosen from the population of high-velocity clouds (HVCs) detected out to 50 kpc projected radius of the Andromeda Galaxy by Thilker et al. (2004, ApJ, 601, L39) with the Green Bank Telescope. Nine pointings were observed with the Westerbork Synthesis Radio Telescope to determine the physical parameters of these objects and to find clues to their origin. One additional pointing was directed at a similar object near M 33.
At 2′ resolution we detect 16 individual HVCs around M 31 and 1 HVC near M 33 with typical H I masses of a few times $10^5\,M_\odot$ and sizes of the order of 1 kpc. Estimates of the dynamical and virial masses of some of the HVCs indicate that they are likely gravitationally dominated by additional mass components such as dark matter or ionised gas. Twelve of the clouds are concentrated in an area of only $1^\circ \times 1^\circ$ at a projected separation of less than 15 kpc from the disk of M 31. This HVC complex has a rather complicated morphological and kinematical structure and partly overlaps with the giant stellar stream of M 31, suggesting a tidal origin. Another detected feature is in close proximity, in both position and velocity, with NGC 205, perhaps also indicative of tidal processes. Other HVCs in our survey are isolated and might represent primordial, dark-matter dominated clouds.

Key words. ISM: clouds – galaxies: local group – galaxies: individual: M 31 – galaxies: individual: M 33 – galaxies: evolution – cosmology: dark matter

1. Introduction

High-velocity clouds (HVCs) were discovered by Muller et al. (1963) in the 21-cm line emission of neutral atomic hydrogen. They are identified by their peculiar radial velocities which are incompatible with participation in the normal rotation of our Galaxy. HVCs can be found all across the sky in a variety of different sizes and shapes (Wakker & van Woerden 1997). Some HVCs form large and coherent complexes spanning tens of degrees in size. Others are comparatively small and isolated. The origin of HVCs is still under debate. In the decades since their discovery many different mechanism have been proposed to explain the observed population of HVCs (see Wakker & van Woerden 1997, for a detailed review). One of the most prominent hypotheses puts forward the Galactic fountain (Shapiro & Field 1976) as a means of forming HVCs. In this scenario, hot gas ejected by the Galactic fountain would cool down and recombine high above the Galactic plane. The condensed gas clouds, falling back ballistically towards the Galactic plane, would then appear as neutral high-velocity clouds. Other scenarios suggest that the gas of HVCs was torn out of dwarf galaxies during close encounters with the Milky Way by tidal forces or by ram-pressure interaction. At least two prominent structures classified as HVCs, the Magellanic Stream (Mathewson et al. 1974) and the Leading Arm (Gardiner & Noguchi 1996; Putman et al. 1998), were formed in this way.

Another hypothesis that has been discussed extensively in recent years postulates that HVCs are primordial gas clouds left over from the formation of the galaxies in the Local Group. This scenario was first suggested by Oort (1966) and recently revived in the framework of cold dark matter (CDM) cosmology by Blitz et al. (1999), who found the kinematic properties of most HVCs to be consistent with a distribution throughout the entire Local Group. They proposed that HVCs might represent the gaseous counterparts of the so-called "missing" dark matter satellites which were predicted by CDM structure formation scenarios (Klypin et al. 1999; Moore et al. 1999; Kravtsov et al. 2004). On the basis of the Leiden/Dwingeloo Survey (LDS) of Galactic neutral hydrogen (Hartmann & Burton 1997) Braun & Burton (1999) identified a sub-sample of 66 compact high-velocity clouds (CHVCs) with angular sizes of less than 2°. The kinematic parameters of the CHVCs suggested an unvirialized population within the Local Group

potential with distances that might extend to the turn-around radius of about 1 Mpc, representing the primordial dark-matter mini-haloes which have not yet been accreted by one of the large galaxies.

Recent observations have raised doubt on an extended Local Group scenario. If the observed CHVC population had a typical distance as large as 1 Mpc, implying a typical H I mass of $10^8\,M_\odot$, then we would expect to detect a similar population of H I clouds in other galaxy groups. However, all attempts to detect such an intra-group population in nearby galaxy groups, employing H I mass limits of about $10^7\,M_\odot$, have failed (Zwaan 2001; Braun & Burton 2001; Pisano et al. 2004). In addition, Hα observations towards a number of CHVCs (Tufte et al. 2002; Putman et al. 2003) have been interpreted to imply distances of the order of only 10 kpc from the Galaxy, where the Galactic radiation field is strong enough to account for the detected Hα intensities. All these observations suggest that the CHVCs are distributed throughout the circum-Galactic environment, more closely associated with the Milky Way rather than being concentrated near the Local Group turn-around radius.

The closest large spiral galaxy comparable to the Milky Way is the Andromeda galaxy (M 31), making it an ideal target to verify the circum-galactic nature of high-velocity clouds observationally. Thilker et al. (2004) used the Green Bank telescope (GBT) to observe a field of $7^\circ \times 7^\circ$ around M 31 in the 21-cm line of neutral hydrogen. They discovered a population of H I clouds (with H I masses between 10^5 and $10^6\,M_\odot$, in the case of Davies' Cloud about $10^7\,M_\odot$) which are likely to be the counterparts of the high-velocity clouds around our Milky Way. A similar GBT survey of a $5^\circ \times 5^\circ$ field around M 33 by Thilker et al. (in prep.) covered another anomalous-velocity H I cloud close to the disk of M 33. This cloud was already described by Huchtmeier (1978) and has properties similar to the HVCs found in the direction of M 31. Many of the clouds in the direction of M 31 and M 33 are rather compact and barely resolved with the GBT. Moreover, complex line profiles in some directions indicate the presence of compact substructure which is unresolved in the GBT data. Therefore, we re-observed some of the HVCs near M 31 and M 33 in H I, using the Westerbork Synthesis Radio Telescope (WSRT). The aim of our interferometric observations was to study the HVCs and their compact substructure with higher angular resolution and to determine their physical parameters.

In this paper we present the results of these WSRT observations and discuss the various possible origins of the detected HVCs in the neighbourhood of M 31 and M 33. After describing the sample selection in Sect. 2, we specify the technical parameters of the observations and the data reduction procedure in Sect. 3. In Sect. 4 the results of our observations are presented. A discussion of our results and their implications can be found in Sect. 5. Finally, Sect. 6 gives a summary of our results and conclusions.

2. Sample selection

Based on the GBT observations of Thilker et al. (2004) and Thilker et al. (in preparation) we selected 9 fields around M 31 and 1 field near M 33 for follow-up observations of HVCs with the WSRT. The 9 fields around M 31 were centred on the brightest and most conspicuous clouds and cover about half of the population of HVCs discovered by Thilker et al. (2004). The targets cover the different morphological types found in the GBT data and include HVCs with both large and small angular separations from the disk of M 31. The most prominent cloud near M 31, Davies' Cloud, was already studied in great detail (Davies 1975; de Heij et al. 2002) so we did not include it in our survey. An overview of the 9 fields around M 31 can be found in Fig. 1.

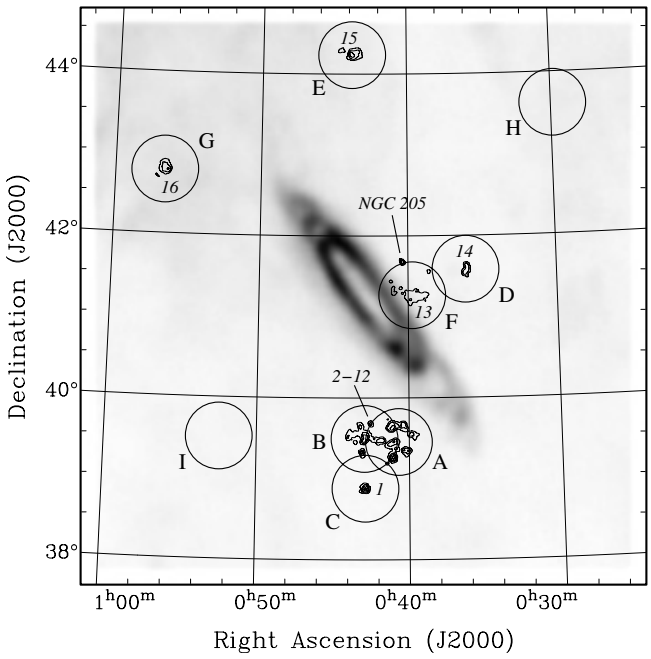

Fig. 1. Overview of the 9 fields (black circles, labelled with capital letters) observed around M 31 with the WSRT. The grayscale image displays the H I emission of M 31 observed by Thilker et al. (2004) with the GBT. The contours show our H I data of the 16 high-velocity clouds detected with the WSRT (labelled with numbers) and of NGC 205. In fields H and I no reliable signal of high-velocity H I emission was found at the resolution and sensitivity of our WSRT data.

The field near M 33 is located about 1° south of the centre of the galaxy. It is centred on a faint H I cloud outside the disk of M 33 which is prominent in the GBT data. The cloud is not isolated but appears to be connected with the H I disk of M 33 by a faint gas bridge.

3. Observations and data reduction

The 10 selected fields were observed in the 21-cm line emission of H I, using the WSRT in the Maxi-Short configuration. This configuration provides particularly good sampling of the shortest East-West baselines (36, 54, 72 and 90 m). A complete 12-h track for each field was preceded and followed by observations of the external calibrator sources CTD93 and 3C 147. The correlator provided 1024 spectral channels for each of the two linear polarisations. To improve the signal-to-noise ratio, the 1024 channels were equally divided among

Table 1. Physical parameters of the high-velocity clouds found near M 31 and M 33. The columns give the cloud name, the right ascension α and declination δ, the peak column density $N_{\rm HI}$ at 2′ resolution, the heliocentric radial velocity $v_{\rm hel}$, the average line width (*FWHM*) of the H I lines Δv, the cloud diameter D (*FWHM*), the H I mass $M_{\rm HI}$, the H I mass in the GBT data of Thilker et al. (2004) $M_{\rm HI}^{\rm GBT}$, the dynamical mass $M_{\rm dyn}$, the virial mass $M_{\rm vir}$, the average H I volume density $n_{\rm HI}$, the value of the velocity gradient δv, the position angle of the velocity gradient φ (measured in the mathematically negative sense with 0° being north), and the ellipticity e. Distances of 780 kpc for M 31 and 800 kpc for M 33 were assumed for the clouds to calculate their sizes, masses, and densities. In the last two rows we have calculated the mean value $\langle x \rangle$ and the standard deviation σ_x of some parameters of M 31 HVCs 1–16.

Cloud name	α (J2000)	δ (J2000)	$N_{\rm HI}$ (10^{19} cm^{-2})	$v_{\rm hel}$ (km s^{-1})	Δv	D (kpc)	$M_{\rm HI}$ ($10^5\,M_\odot$)	$M_{\rm HI}^{\rm GBT}$	$M_{\rm dyn}$ ($10^5\,M_\odot$)	$M_{\rm vir}$	$n_{\rm HI}$ (10^{-2} cm^{-3})	δv (km s^{-1} kpc^{-1})	φ (°)	e
M 31 HVC 1	$0^{\rm h}42^{\rm m}53^{\rm s}$	38°52′	11.1	−503	17.3	0.72	5.2	4.8	>86	230	10.9	7.7	349	0.24
M 31 HVC 2	$0^{\rm h}41^{\rm m}03^{\rm s}$	39°16′	9.5	−511	29.6	0.75	5.0		>44	690	9.3	9.7	188	0.12
M 31 HVC 3	$0^{\rm h}40^{\rm m}11^{\rm s}$	39°21′	3.4	−509	18.5	0.93	2.2			330	2.1	8.4	239	0.28
M 31 HVC 4	$0^{\rm h}43^{\rm m}07^{\rm s}$	39°20′	4.2	−518	21.0	0.56	1.3			260	5.8	4.1	98	0.22
M 31 HVC 5	$0^{\rm h}42^{\rm m}51^{\rm s}$	39°31′	5.8	−512	25.3	1.13	6.0				3.3			0.48
M 31 HVC 6	$0^{\rm h}42^{\rm m}31^{\rm s}$	39°41′	1.8	−517	17.3	0.53	0.6		>19	170	3.2	4.1	334	0.42
M 31 HVC 7	$0^{\rm h}41^{\rm m}03^{\rm s}$	39°26′	3.7	−464	20.3	1.27	3.5				1.3	10.7	280	0.40
M 31 HVC 8	$0^{\rm h}41^{\rm m}47^{\rm s}$	39°28′	3.0	−476	32.1	0.92	2.1		>730		2.1	15.5	291	0.36
M 31 HVC 9	$0^{\rm h}43^{\rm m}13^{\rm s}$	39°39′	1.8	−448	19.1	0.69	0.8			260	1.9	12.7	252	0.51
M 31 HVC 10	$0^{\rm h}41^{\rm m}03^{\rm s}$	39°38′	3.9	−432	30.2	1.20	5.0		>810		2.3	14.7	262	0.38
M 31 HVC 11	$0^{\rm h}43^{\rm m}32^{\rm s}$	39°27′	0.9	−454	30.2	0.43	0.2			410	2.0			0.26
M 31 HVC 12	$0^{\rm h}43^{\rm m}49^{\rm s}$	39°33′	1.3	−390	30.8	1.5	1.5				0.3			
M 31 HVC 13	$0^{\rm h}39^{\rm m}35^{\rm s}$	41°15′	1.3	−211	22.8	2.6	3.5	8.7			0.2	4.6	233	0.65
M 31 HVC 14	$0^{\rm h}36^{\rm m}04^{\rm s}$	41°34′	2.9	−512	24.0	1.11	2.5	3.0			1.4			0.61
M 31 HVC 15	$0^{\rm h}43^{\rm m}50^{\rm s}$	44°14′	4.8	−273	26.5	1.07	5.2	5.2		790	3.3	4.5	176	0.37
M 31 HVC 16	$0^{\rm h}56^{\rm m}25^{\rm s}$	42°47′	3.4	−164	25.9	1.26	3.9	4.4		890	1.5	8.9	115	0.43
M 31 HVC A	$0^{\rm h}40^{\rm m}23^{\rm s}$	39°41′	2.5	−455	32.1	1.04	1.9				1.3			0.56
M 31 HVC B	$0^{\rm h}39^{\rm m}54^{\rm s}$	39°33′	1.9	−468	39.5	0.91	1.3				1.3			0.57
M 33 HVC 1	$1^{\rm h}32^{\rm m}33^{\rm s}$	29°34′	5.2	−147	17.3	1.33	7.8				2.6			0.43
$\langle x \rangle$			3.9		24.4	1.04	3.0			450	3.2	8.8		0.38
σ_x			±2.8		±5.1	±0.52	±1.9			±270	±3.0	±4.1		±0.15

two independent IF bands tuned to the same central frequency, resulting in 512 channels for the final spectrum. By later averaging these two IF bands we are able to decrease the digitization noise by a factor $\sqrt{2}$. As a result, the noise level in the final images is about 5% lower in comparison with the normal single-IF mode. With a bandwidth of 5 MHz the corresponding velocity resolution is about 2 km s^{-1}.

The data reduction was done with the AIPS software package. After flagging the data affected by radio frequency interference or by shadowing of the telescopes we carried out the standard bandpass, gain, and flux calibration, using the two external calibrators. To further improve the gain calibration, we self-calibrated on the continuum sources in each field in an iterative procedure. This provided us with a clean component model of the continuum emission which was then subtracted from the visibility data.

As the emission of most HVCs in our survey was quite faint and extended, we applied a Gaussian *uv* taper, declining to 30% amplitude at 1.25 kλ radius, before producing the final, cleaned images. The resulting synthesised beam has a *FWHM* of about 2′, corresponding to a spatial resolution of about 450 pc at the distance of M 31. For the brightest and most compact clouds we also produced images with a higher angular resolution of 30″ *FWHM* (using a *uv* taper radius of 5 kλ). The velocity resolution was also smoothed to 12 km s^{-1} in all spectra to further increase the signal-to-noise ratio, given that the typical detected linewidth was about 25 km s^{-1}. For the 2′ resolution maps, at 12 km s^{-1}, we obtain an rms sensitivity of about 1 mJy/beam towards the centre of the field, corresponding to a brightness temperature rms of 40 mK. This implies a 1σ H I column density sensitivity of 9×10^{17} cm^{-2} for emission filling the 2′ beam.

4. Results

In two of the nine fields around M 31 no high-velocity gas was detected. In both cases the emission of the high-velocity gas is probably too faint and/or diffuse to be detected in our WSRT data given the finite column density sensitivity noted above (9×10^{17} cm^{-2} over 12 km s^{-1}). In all other fields we clearly detect the HVCs at more than 5σ significance. The individual clouds have been named M*xy* HVC *z*, where *xy* is the Messier number of the host galaxy and *z* is the catalogue number assigned to each HVC.

The observational parameters of all clouds are summarised in Table 1. Under the assumption of a constant distance of 780 kpc (Stanek & Garnavich 1998) we obtain a mean linear size of the 16 HVCs around M 31 of about 1 kpc *FWHM* and

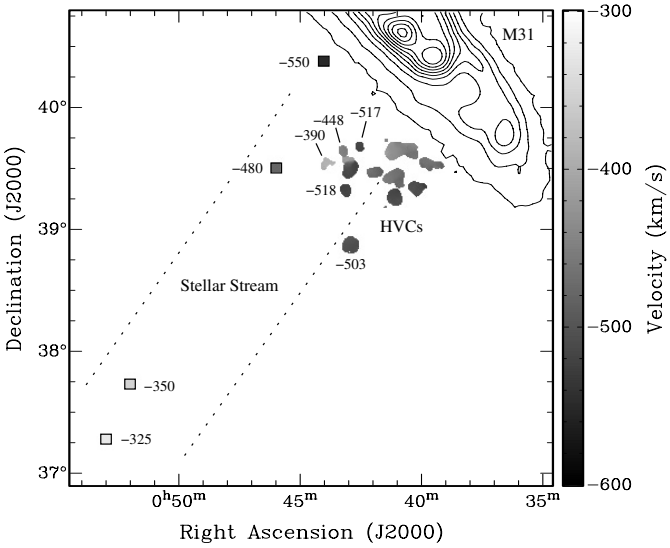

Fig. 2. The map compares the position and heliocentric velocitiy of the giant stellar stream of M 31 with the nearby high-velocity clouds. The squares indicate the positions of the radial velocity measurements along the stream (outlined by the dotted lines) by Ferguson et al. (2004). For comparison we have inserted the first moment maps of the HVCs from our data. The GBT data of the H I disk of M 31 from Thilker et al. (2004) is shown for orientation in black contours in the upper right corner of the map. The numbers denote the heliocentric radial velocities of individual features.

a mean H I mass of $3 \times 10^5\,M_\odot$. For the HVC near M 33 we assumed a distance of 800 kpc (Lee et al. 2002) to determine the physical parameters.

The H I column densities were derived from the zeroth moment of the spectra under the assumption that the optical depth of the gas is negligible. From the integrated column density $N_{\rm HI}^{\rm tot}$ we can directly calculate the H I mass of each cloud via $M_{\rm HI} = m_{\rm H}\,d^2\tan^2\varphi\,N_{\rm HI}^{\rm tot}$, where $m_{\rm H}$ is the mass of a hydrogen atom, d is the distance of the cloud, and φ denotes the angular size of a resolution element of the map. The observed H I masses are in the range of a few times $10^4\,M_\odot$ to $6\times10^5\,M_\odot$. For the isolated clouds in the direction of M 31 we have also listed in Table 1 the H I masses derived from the GBT data of Thilker et al. (2004). These values are in good agreement with our WSRT observations. Only for the most extended and diffuse cloud, M 31 HVC 13, we detect only about 40% of the total flux.

The diameters of the HVCs were determined by fitting a Gaussian to the radial column density distribution. By dividing the H I mass by the volume defined by the *FWHM* of this Gaussian, we can estimate a mean H I volume density $n_{\rm HI}$ for each cloud under the additional assumption of spherical symmetry. The derived densities are typically of the order of a few times 10^{-2} cm^{-3}. These volume densities are between two and three orders of magnitude higher than the densities of $10^{-5}\ldots10^{-4}$ cm^{-3} expected for an extended galactic corona in which the HVCs might be embedded (Sembach et al. 2003; Rasmussen et al. 2003).

The mean radial velocities of the HVCs were calculated from the first moment of the spectra. Most values are more negative than the M 31 systemic velocity of $v_{\rm hel} \approx -300$ km s^{-1}. However, this is a selection effect, because most of the HVCs detected around M 31 belong to a filamentary complex of clouds with similar radial velocities near the southern edge of the galaxy. The HVC near M 33 has a slightly less negative radial velocity with respect to the M 33 systemic velocity of $v_{\rm hel} \approx -180$ km s^{-1}. By fitting a Gaussian to the spectral lines we extracted the line widths with typical values in the range of about $20\ldots30$ km s^{-1} *FWHM* at $2'$ resolution. These values correspond to an upper limit for the kinetic temperature of the gas of the order of 10^4 K. Similar line widths are observed for the Galactic HVCs (e.g. Wakker & van Woerden 1997; Braun & Burton 1999; Westmeier et al. 2005b), and they are typical for the warm neutral medium (Braun 1997). Thilker et al. (2004) already noted that the large line widths of the HVCs discovered in the GBT survey of M 31 require a large fraction of undetected mass to allow for gravitational stability of the clouds. We address this problem in more detail in the discussion in Sect. 5.1.

We also determined the radial velocity gradients across some of the HVCs by fitting a plane $P(x,y) = cx + dy + f$ to the first moment maps $v_{\rm hel}(x,y)$. The chi-square minimisation provided us with values for the parameters c, d and f from which we calculated the absolute value $\delta v = \sqrt{c^2+d^2}$ and the direction $\varphi = 90^\circ - \arctan(d/c)$ of the velocity gradient. In this definition the position angle, φ, is measured in the usual (east of north) sense. The velocity gradients are listed in Table 1 for those clouds where a meaningful fit could be obtained. The method, of course, only provides us with a linear approximation of an average global velocity gradient across each cloud, whereas the observed gradients are not expected to be perfectly linear and, on the local scale, will deviate from the average value and direction determined from the planar fits.

The ellipticities of the HVCs were obtained by fitting an ellipse to the column density distribution. The parameters of the ellipse were derived from a weighted second moment analysis, following the procedure described by Banks et al. (1995). The ellipse centre was fixed by the first moment of the column density distribution. From the calculation of the second moments we then derived the major and minor axis, a and b, of the ellipse. The ellipticities given in Table 1 are defined by $e = 1 - \frac{b}{a}$. Only M 31 HVC 12 was so diffuse and extended that a meaningful fit could not be obtained.

4.1. M 31 HVC 1

M 31 HVC 1 is located about half a degree south of M 31 HVCs 2–12. This proximity together with similar radial velocities suggests a connection with M 31 HVCs 2–12. M 31 HVC 1 reveals the highest peak column density detected among all clouds in our sample with $N_{\rm HI} = 1.1\times10^{20}$ cm^{-2} at $2'$ resolution. The H I mass is $M_{\rm HI} = 5\times10^5\,M_\odot$. Maps and profiles of the cloud are presented in Fig. 4. At first glance, M 31 HVC 1 has a spherically-symmetric appearance. Furthermore, it shows a systematic radial velocity gradient, measuring about 15 km s^{-1} in an approximately north-south direction. The high brightness of M 31 HVC 1 allowed us to

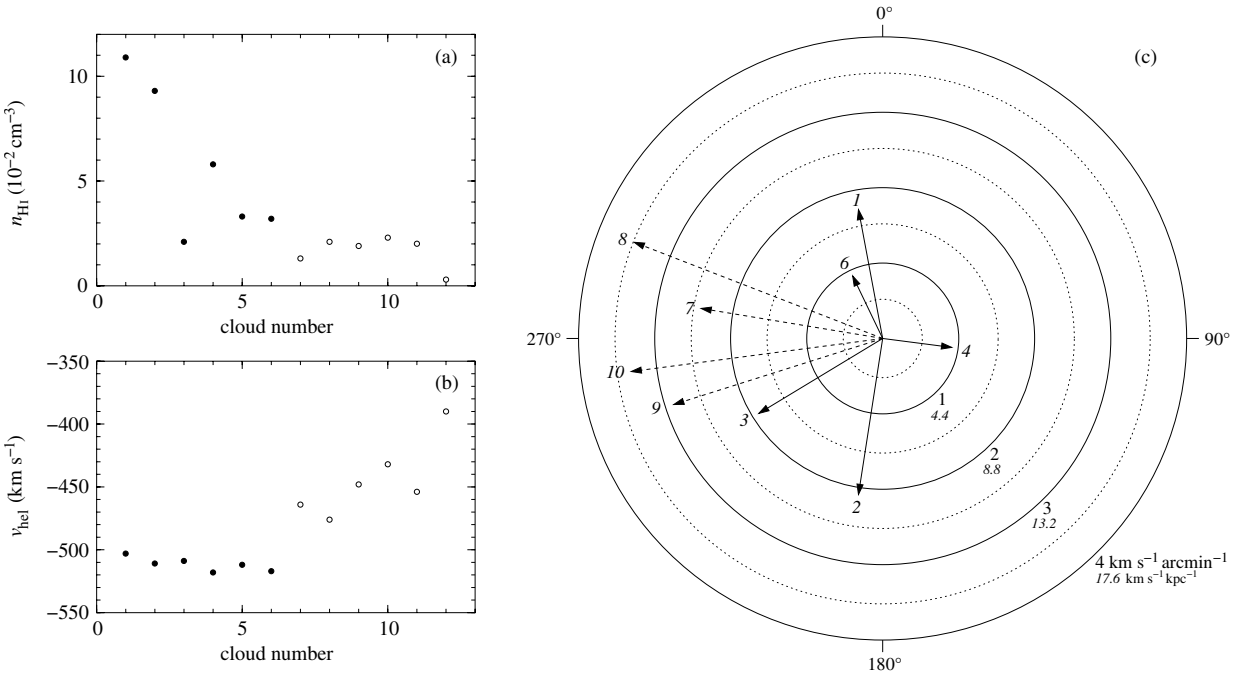

Fig. 3. a) H I volume densities n_{HI} and **b)** heliocentric radial velocities v_{hel} of M 31 HVCs 1–12. M 31 HVCs 1–6 (•) have similar radial velocities, and they are much more condensed with typically higher densities. M 31 HVCs 7–12 (○), in contrast, are more diffuse with lower densities and rather different radial velocities. In **c)** we have plotted the value of the velocity gradient across some of the clouds (labelled with italic numbers) in km s^{-1} arcmin^{-1} (labelled from 1 to 4) against the direction of the gradient in degrees. It turns out that the gradients across M 31 HVCs 1–6 (solid arrows) have arbitrary orientations whereas the typically larger gradients across M 31 HVCs 7–10 (dashed arrows) are all oriented in about the same direction. Note that for M 31 HVCs 5, 11, and 12 we could not obtain a meaningful fit for the velocity gradient.

additionally generate a map with 30″ angular resolution which is shown in Fig. 15. The high-resolution column density map resolves M 31 HVC 1 into a fairly compact core with a peak column density of more than 2×10^{20} cm^{-2} which is embedded in a more diffuse envelope with a conspicuous extension in the northern direction. We also produced a data cube with higher velocity resolution which shows that the spectral lines in the direction of the core have significantly smaller line widths of only about 6 km s^{-1}, indicating the presence of cold gas in the core.

4.2. M 31 HVCs 2–12

M 31 HVCs 2–12 are probably the most remarkable feature detected in our survey. They are crowded in an area in the sky of about 1° in size, and they are located in projection close to the edge of the H I disk of M 31. An overview of the whole field is shown in Fig. 5 while maps and profiles of some individual clouds are presented in Figs. 6–9. Maps with 30″ resolution of some of the HVCs are shown in Figs. 15 and 16. The individual clouds in this complex of HVCs appear to be arranged in filaments intersecting each other at different angles. The radial velocities of the clouds cover a very large range of -520 km s^{-1} $\lesssim v_{hel} \lesssim -390$ km s^{-1}, and it looks as if clouds along the apparent filaments have similar radial velocities.

There also appears to be a morphological distinction between some of the filaments. M 31 HVCs 2–6 (and also HVC 1 which is presumably associated with the HVC complex) have very similar radial velocities of $v_{hel} \approx -520 \ldots -500$ km s^{-1}. Furthermore, they all show high peak fluxes and mean volume densities as well as being fairly condensed. M 31 HVCs 7–12, in contrast, have different radial velocities of $v_{hel} \approx -480 \ldots -390$ km s^{-1}, and they are more diffuse with typically lower peak fluxes and densities. The average H I volume densities and the heliocentric radial velocities of the 12 HVCs are plotted in Figs. 3a and b. A distinction between the two different groups of HVCs in this area can also be made on the basis of the velocity gradients observed across the clouds. While the velocity gradients across M 31 HVCs 1–6 have arbitrary orientations, the somewhat larger gradients observed across M 31 HVCs 7–12 appear to be oriented in the same direction (see Fig. 3c).

Two other clouds at the north-western edge of the map have been named M 31 HVC A and B. Both are fairly diffuse with only moderate H I peak column densities and relatively broad spectral lines which distinguishes them from the HVCs discussed before. The radial velocities along the two clouds seem to follow those observed for the H I disk of M 31 which was also covered at the edge of our field of view and which can partly be seen in the upper-right corner of the column density map in Fig. 5. This suggests that M 31 HVC A and B might represent gas of an outer disk component of M 31.

4.3. M 31 HVC 13

M 31 HVC 13 is rather diffuse and extended. It has quite low column densities and appears to be fragmented into smaller clumps towards the eastern edge. Maps and profiles are shown

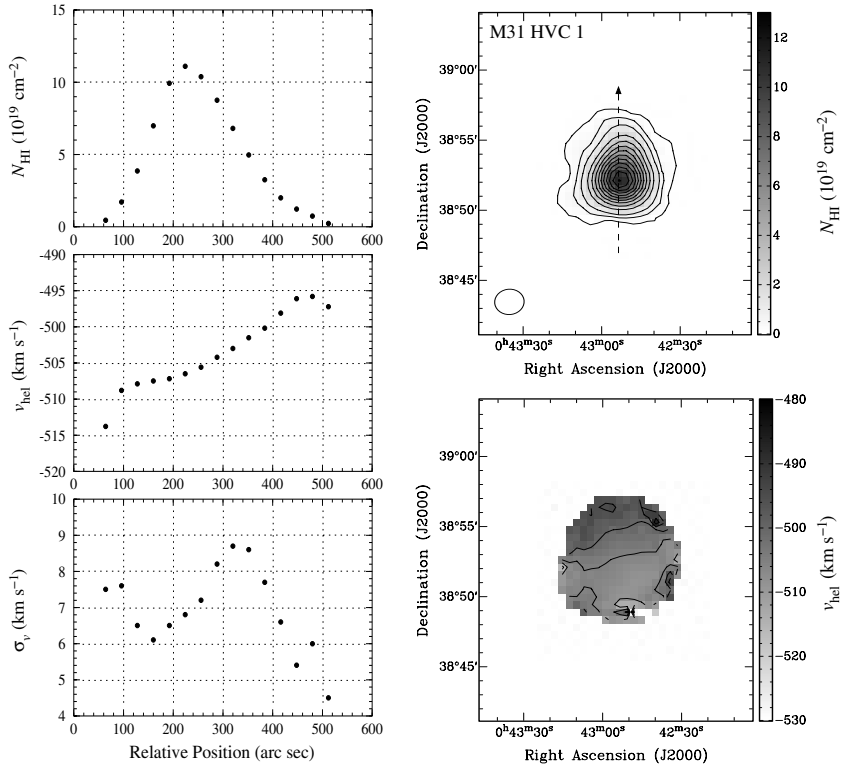

Fig. 4. M 31 HVC 1. *The upper right map* displays the H I column density. The contours are drawn at 1×10^{18} cm^{-2}, 5×10^{18} cm^{-2}, and from 1×10^{19} cm^{-2} in steps of 1×10^{19} cm^{-2}. *The lower right map* shows the heliocentric radial velocity. The contours are separated by 5 km s^{-1}. The diagrams on the left hand side show *from top to bottom*: the H I column density, the heliocentric radial velocity, and the velocity dispersion of the gas along the cut marked by the arrow in the column density map.

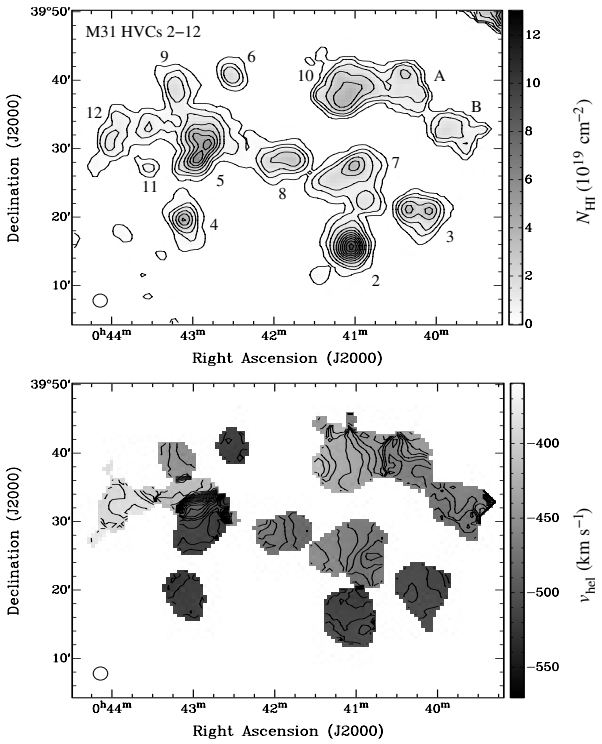

Fig. 5. Map of the H I column densities (*top*) and the heliocentric radial velocities (*bottom*) of M 31 HVCs 2–12. The contours in the upper map are drawn at 1×10^{18} cm^{-2}, 5×10^{18} cm^{-2} and from 1×10^{19} cm^{-2} in steps of 1×10^{19} cm^{-2}. The contours in the lower map are separated by 5 km s^{-1}.

in Fig. 10. M 31 HVC 13 appears in projection against the H I disk of M 31. But its radial velocity is different by about 130 km s^{-1} from that of the disk gas observed in this direction, so that it is presumably located outside the disk plane of M 31. It lies only about half a degree south of NGC 205, the satellite galaxy of M 31. H I emission from NGC 205 was also detected at the edge of our field of view. Interestingly, the radial velocities of the gas observed in NGC 205 and M 31 HVC 13 cover essentially the same range. Despite the positional and velocity correspondence we do not detect a continuous H I bridge between these two objects at our sensitivity.

4.4. M 31 HVCs 14–16

The remaining three HVCs observed near M 31 are all positionally isolated from each other and from the disk of M 31. Maps and profiles are shown in Figs. 11–13. All three clouds clearly deviate from a spherically-symmetric appearance. While M 31 HVC 14 is elongated and slightly bent, M 31 HVCs 15 and 16 exhibit a pronounced head-tail structure. A compact core appears to be embedded in an asymmetric envelope which forms an extended tail in one direction. Head-tail structures like these are also widely observed in the case of Galactic HVCs (Brüns et al. 2000, 2001; Westmeier et al. 2005b), and they are suggestive of a distortion of the clouds by external forces like e.g. the ram pressure of an ambient medium.

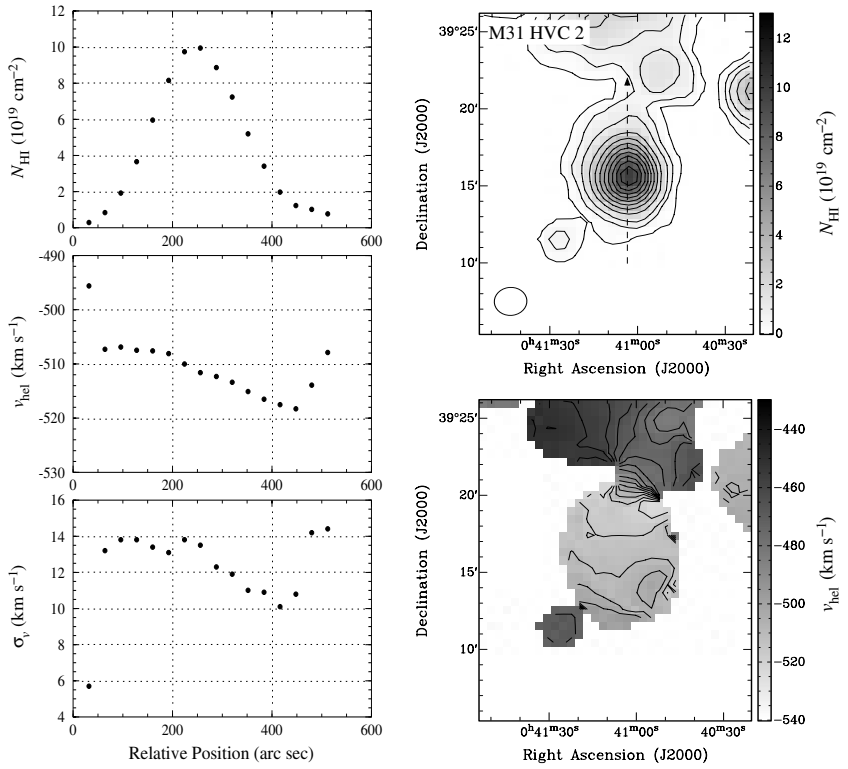

Fig. 6. M 31 HVC 2. *The upper right map* displays the H I column density. The contours are drawn at 1×10^{18} cm^{-2}, 5×10^{18} cm^{-2}, and from 1×10^{19} cm^{-2} in steps of 1×10^{19} cm^{-2}. *The lower right map* shows the heliocentric radial velocity. The contours are separated by 5 km s^{-1}. The diagrams on the left hand side show *from top to bottom*: the H I column density, the heliocentric radial velocity, and the velocity dispersion of the gas along the cut marked by the arrow in the column density map.

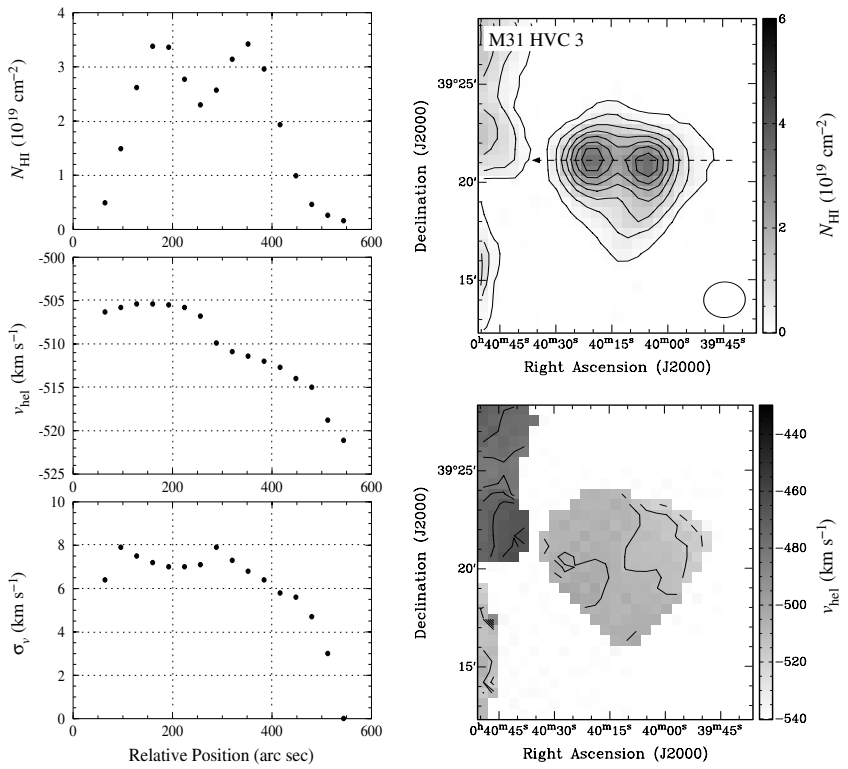

Fig. 7. M 31 HVC 3. *The upper right map* displays the H I column density. The contours are drawn at 1×10^{18} cm^{-2} and from 5×10^{18} cm^{-2} in steps of 5×10^{18} cm^{-2}. *The lower right map* shows the heliocentric radial velocity. The contours are separated by 5 km s^{-1}. The diagrams on the left hand side show *from top to bottom*: the H I column density, the heliocentric radial velocity, and the velocity dispersion of the gas along the cut marked by the arrow in the column density map.

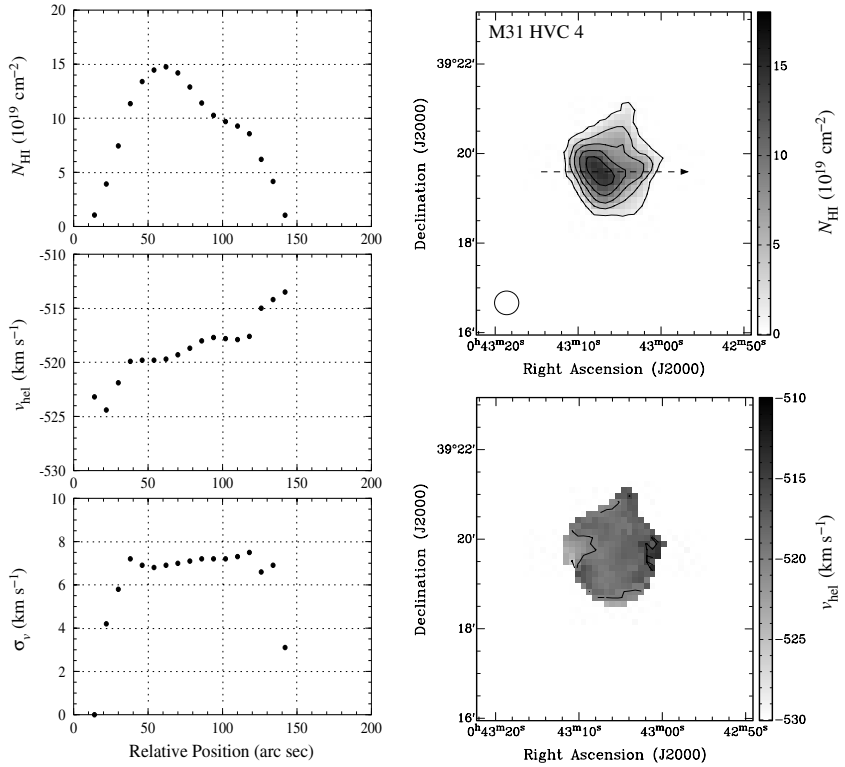

Fig. 8. M 31 HVC 4. *The upper right map* displays the H I column density. The contours are drawn from 1×10^{19} cm^{-2} in steps of 3×10^{19} cm^{-2}. *The lower right map* shows the heliocentric radial velocity. The contours are separated by 5 km s^{-1}. The diagrams on the left hand side show *from top to bottom*: the H I column density, the heliocentric radial velocity, and the velocity dispersion of the gas along the cut marked by the arrow in the column density map.

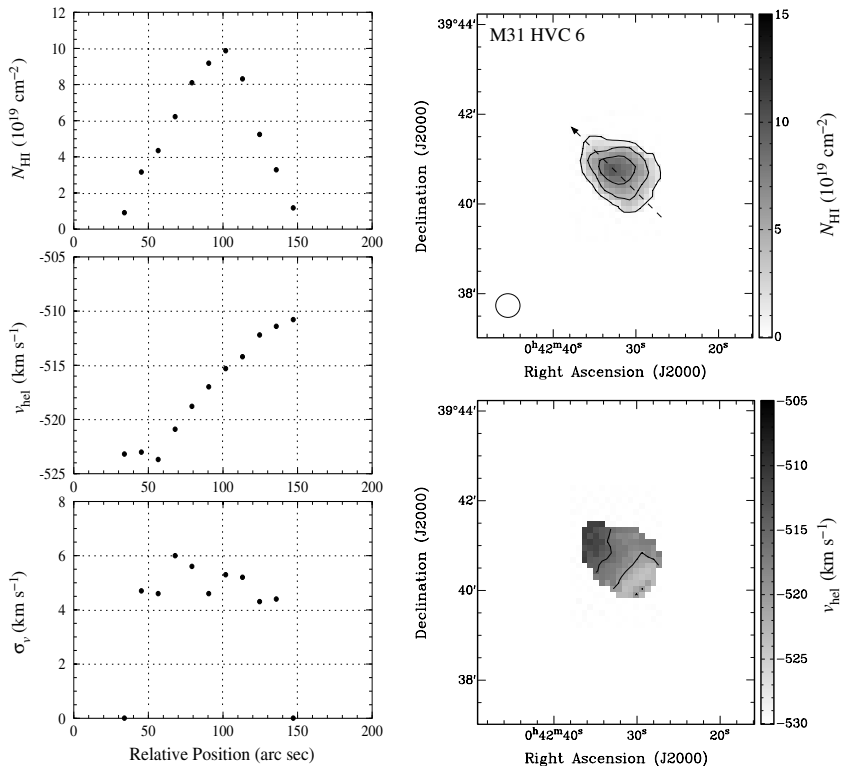

Fig. 9. M 31 HVC 6. The upper right map displays the H I column density. The contours are drawn from 1×10^{19} cm^{-2} in steps of 3×10^{19} cm^{-2}. The lower right map shows the heliocentric radial velocity. The contours are separated by 5 km s^{-1}. The diagrams on the left hand side show *from top to bottom*: the H I column density, the heliocentric radial velocity, and the velocity dispersion of the gas along the cut marked by the arrow in the column density map.

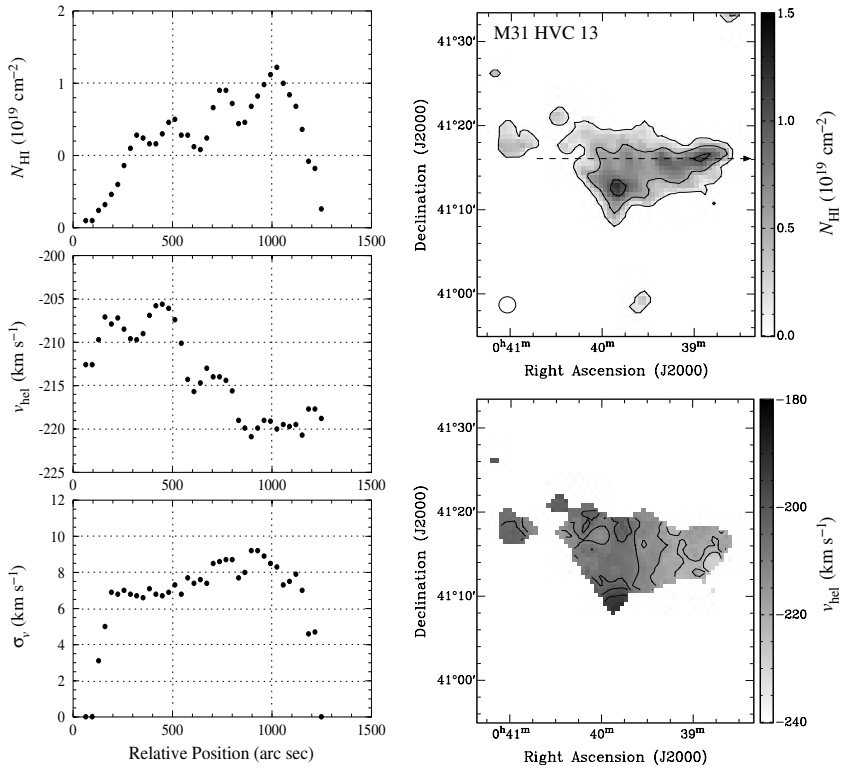

Fig. 10. M 31 HVC 13. *The upper right map* displays the H I column density. The contours are drawn at 1×10^{18} cm^{-2} and from 5×10^{18} cm^{-2} in steps of 5×10^{18} cm^{-2}. *The lower right map* shows the heliocentric radial velocity. The contours are separated by 5 km s^{-1}. The diagrams on the left hand side show *from top to bottom*: the H I column density, the heliocentric radial velocity, and the velocity dispersion of the gas along the cut marked by the arrow in the column density map.

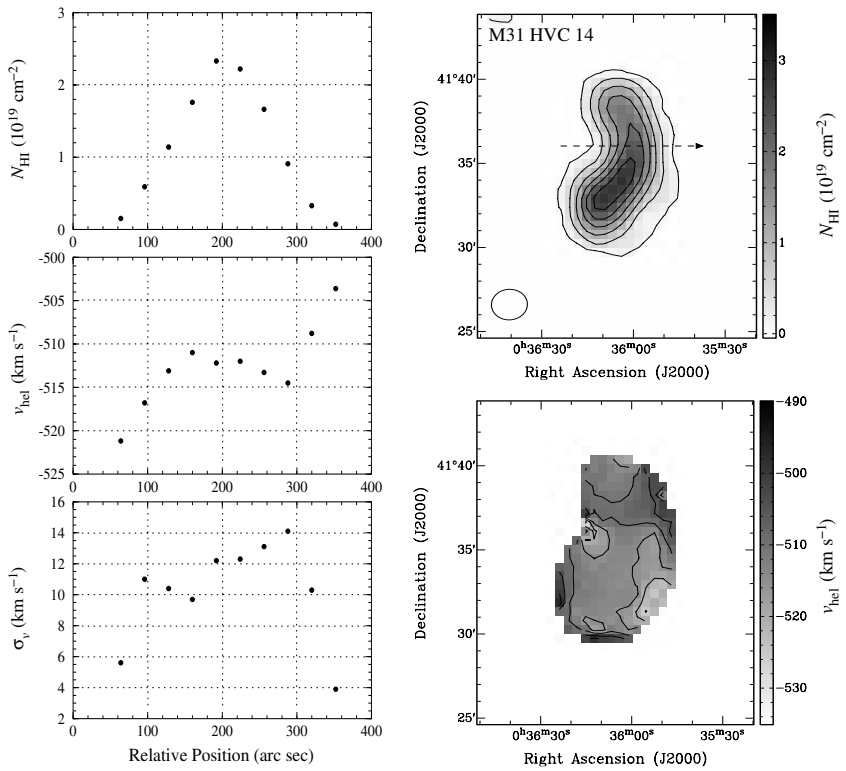

Fig. 11. M 31 HVC 14. *The upper right map* displays the H I column density. The contours are drawn at 1×10^{18} cm^{-2} and from 5×10^{18} cm^{-2} in steps of 5×10^{18} cm^{-2}. *The lower right map* shows the heliocentric radial velocity. The contours are separated by 5 km s^{-1}. The diagrams on the left hand side show *from top to bottom*: the H I column density, the heliocentric radial velocity, and the velocity dispersion of the gas along the cut marked by the arrow in the column density map.

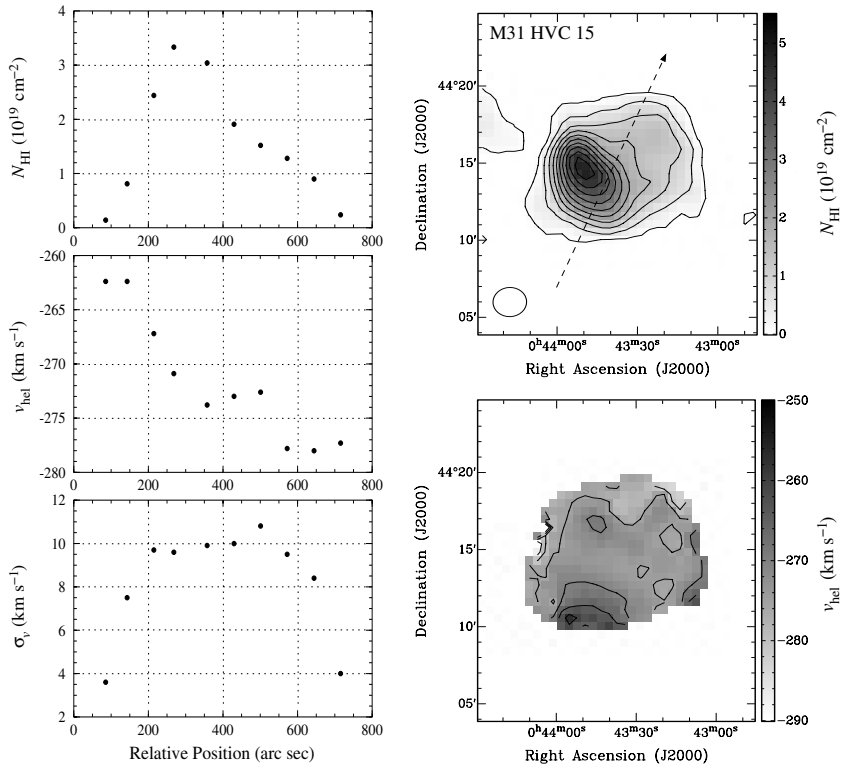

Fig. 12. M 31 HVC 15. *The upper right map* displays the H I column density. The contours are drawn at 1×10^{18} cm^{-2} and from 5×10^{18} cm^{-2} in steps of 5×10^{18} cm^{-2}. *The lower right map* shows the heliocentric radial velocity. The contours are separated by 5 km s^{-1}. The diagrams on the left hand side show *from top to bottom*: the H I column density, the heliocentric radial velocity, and the velocity dispersion of the gas along the cut marked by the arrow in the column density map.

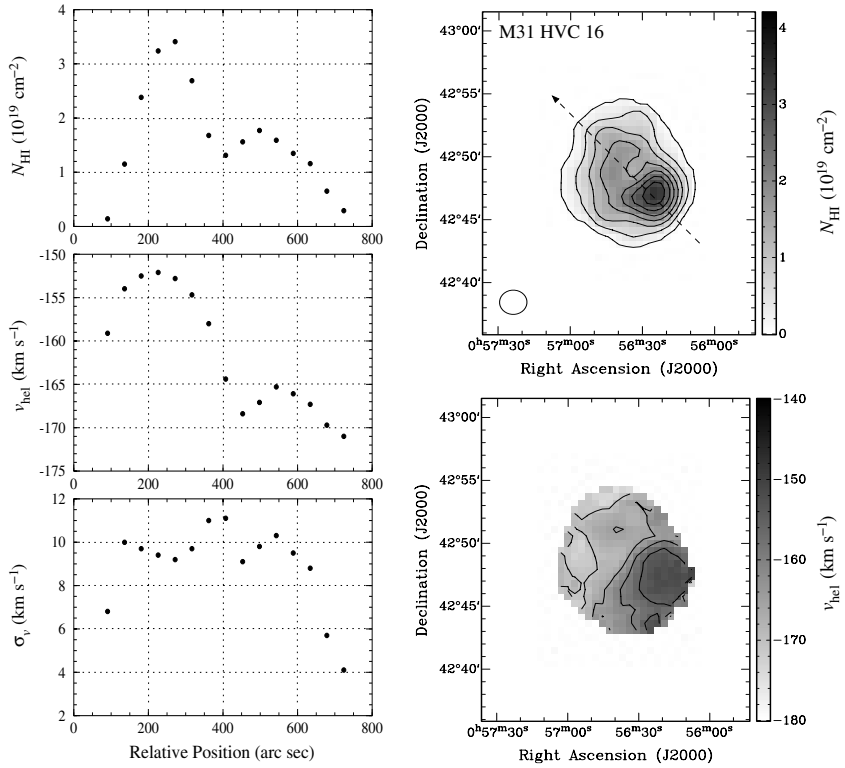

Fig. 13. M 31 HVC 16. *The upper right map* displays the H I column density. The contours are drawn at 1×10^{18} cm^{-2} and from 5×10^{18} cm^{-2} in steps of 5×10^{18} cm^{-2}. *The lower right map* shows the heliocentric radial velocity. The contours are separated by 5 km s^{-1}. The diagrams on the left hand side show *from top to bottom*: the H I column density, the heliocentric radial velocity, and the velocity dispersion of the gas along the cut marked by the arrow in the column density map.

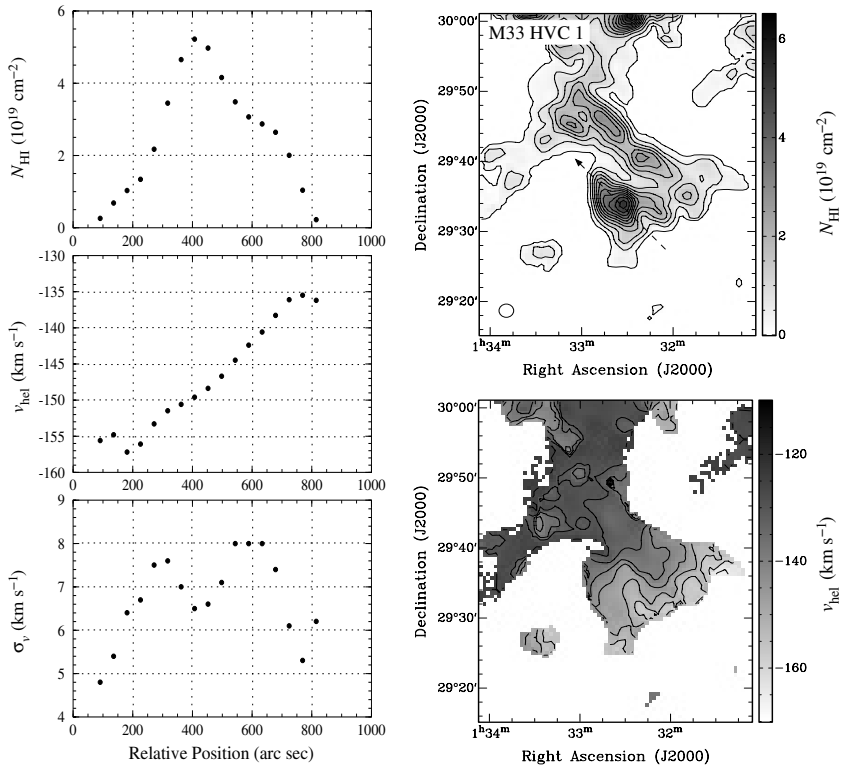

Fig. 14. M 33 HVC 1. *The upper right map* displays the H I column density. The contours are drawn at 1×10^{18} cm^{-2} and from 5×10^{18} cm^{-2} in steps of 5×10^{18} cm^{-2}. *The lower right map* shows the heliocentric radial velocity. The contours are separated by 5 km s^{-1}. The diagrams on the left hand side show *from top to bottom*: the H I column density, the heliocentric radial velocity, and the velocity dispersion of the gas along the cut marked by the arrow in the column density map.

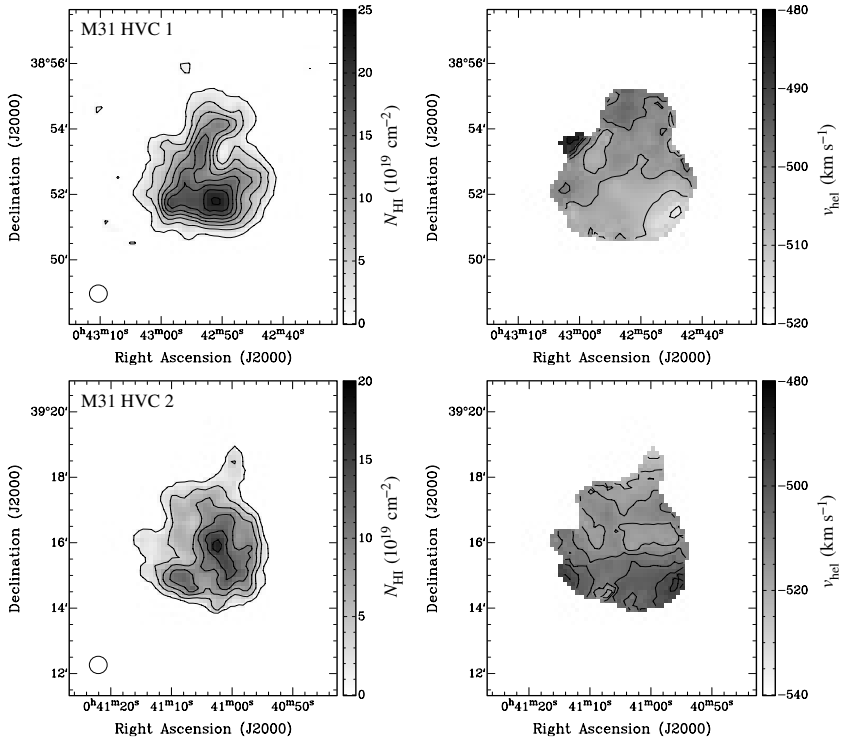

Fig. 15. Maps of the H I column density (*left*) and the heliocentric radial velocity (*right*) of M 31 HVCs 1 and 2 with a higher angular resolution of about 30″. The contours in the column density maps are drawn from 1×10^{19} cm^{-2} in steps of 3×10^{19} cm^{-2}. The contours in the radial velocity maps are drawn in steps of 5 km s^{-1}. Both clouds show compact sub-structure which is not resolved in the 2′ maps.

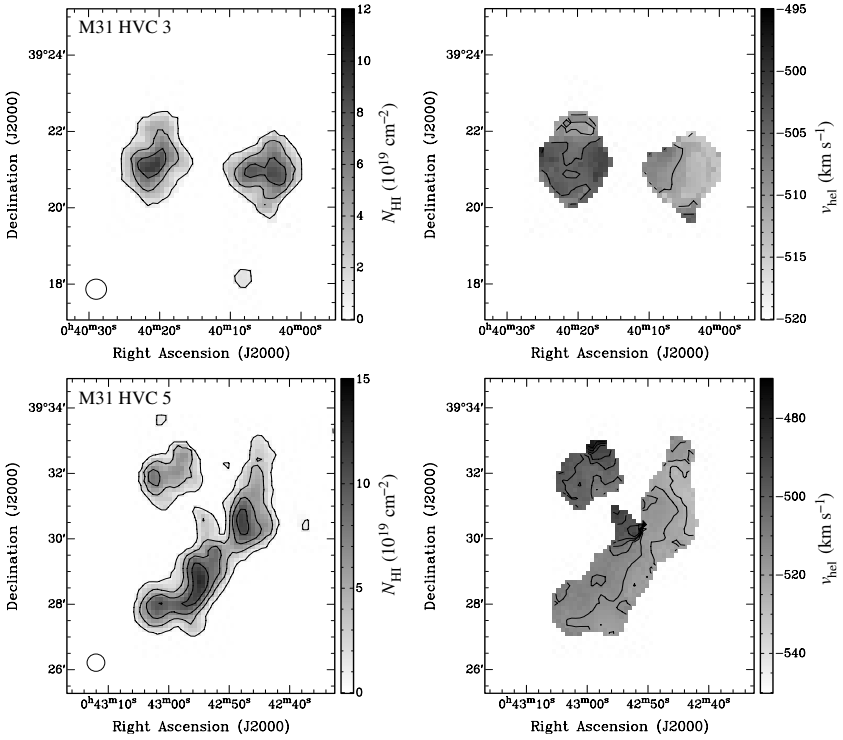

Fig. 16. Maps of the H I column density (*left*) and the heliocentric radial velocity (*right*) of M 31 HVCs 3 and 5 with a higher angular resolution of about 30″. The contours in the column density maps are drawn from 1×10^{19} cm^{-2} in steps of 3×10^{19} cm^{-2}. The contours in the radial velocity maps are drawn in steps of 5 km s^{-1}. Both clouds break up into sub-clumps which are hardly resolved in the 2′ maps.

4.5. M 33 HVC 1

M 33 HVC 1 is located about 1° south of the centre of M 33. It is the most conspicuous HVC around M 33 found in the GBT survey by Thilker et al. (in preparation). In the GBT data it is already obvious that the HVC is not isolated but connected with the H I disk of M 33 by a faint gas bridge. In our WSRT data (Fig. 14) this bridge is very prominent with H I column densities of a few times 10^{19} cm^{-2}. Both M 33 HVC 1 and the gas bridge share a common gradient in radial velocity measuring about 20 km s^{-1}.

5. Discussion

5.1. Dynamical mass and stability

Three clouds, M 31 HVCs 1, 2, and 6, have a spherical appearance combined with a pronounced gradient in radial velocity. Two more clouds, M 31 HVCs 8 and 10, have a pronounced, linear velocity gradient, although they appear slightly elliptical. If we assume these velocity gradients to be caused by a rotation of the clouds we can estimate their dynamical mass

$$M_{\rm dyn} = \frac{R\, v_{\rm rot}^2}{G} \qquad (1)$$

where R is the radius of the cloud, $v_{\rm rot}$ is the rotation velocity at the edge, and G denotes the gravitational constant. The velocity gradients δv over the angular extent ϑ were estimated from the one-dimensional cuts across the clouds and are summarised in Table 2. Because of the unknown inclination angle i of the clouds the observed velocity gradient δv only gives us a lower limit of the rotation velocity with $v_{\rm rot} = \delta v/(2 \cos i)$. Nonetheless, the obtained lower limits for the dynamical masses of the five clouds are already by one or two orders of magnitude larger than the observed H I masses (see Table 1). If the assumption of rotation is correct we are seeing only a small fraction of the clouds' masses in neutral atomic hydrogen. Additional mass components like ionised gas or dark matter are required to account for the observed velocity gradients.

Table 2. Parameters for the determination of the dynamical masses of M 31 HVCs 1, 2, 6, 8, and 10. δv is the observed radial velocity gradient across the angular extent ϑ of each cloud as extracted from the one-dimensional cuts in Figs. 4, 6, and 9 and from the map in Fig. 5. $M_{\rm dyn}$ denotes the lower limit for the derived dynamical mass.

Object	δv (km s^{-1})	ϑ (arcsec)	$M_{\rm dyn}$ (10^5 $M_\odot$)
M 31 HVC 1	14	400	>86
M 31 HVC 2	10	400	>44
M 31 HVC 6	13	100	>19
M 31 HVC 8	35	540	>730
M 31 HVC 10	37	540	>810

A similar result can be derived by applying the virial theorem, assuming spherical symmetry and, for simplicity, a constant mass density. We can justify the assumption of virialisation by making a simple estimate of the dynamical timescales of the clouds. If we consider the mean diameter of the clouds to be $D \approx 1$ kpc and the mean *FWHM* of the spectral lines to be $\Delta v \approx 25$ km s^{-1} we obtain an estimate for the dynamical

timescale of $\tau_{\rm dyn} = D/\Delta v \approx 4 \times 10^7$ yr. This timescale is short compared with the expected orbital timescales of the HVCs relative to M 31, about 10^9 yr, over which changing tidal forces might be active. Thus, we can assume that the HVCs are at least close to internal dynamical equilibrium so that we can apply the virial theorem which, in our case, reads

$$\frac{\Delta v^2}{8 \ln 2} = \frac{G M_{\rm vir}}{5R}. \quad (2)$$

Here, $M_{\rm vir}$ is the virial mass of the cloud, R is the cloud radius, G denotes the gravitational constant, and Δv is the *FWHM* of the H I lines. Solving Eq. (2) for the virial mass and inserting the parameters given in Table 1 yields virial masses of the order of a few times $10^7\,M_\odot$ for the most condensed clouds in our sample. The calculated virial masses lead to a typical mass fraction of neutral hydrogen of less than 1%. Although these are small values, we have to consider that the observed line widths are probably only upper limits for the velocity dispersion of the gas since internal kinematics or turbulence can result in an additional broadening of the spectral lines.

It should also be stressed that the application of the virial theorem to H I clouds is open to justified criticism. Not only does the calculation of virial masses depend upon a number of assumptions with respect to the object symmetry, but the simple form of Eq. (2) also demands a homogeneous population of particles with identical masses. It is doubtful that the velocity dispersion of the H I component alone would provide a realistic estimate of the total mass of HVCs. Moreover, the calculation of dynamical masses according to Eq. (1) is in conflict with the virial theorem in the form of Eq. (2). The virial theorem requires random motions of the particles instead of a regular rotation of the cloud. Either the dynamical mass or the virial mass of a particular cloud can be correct but not both. By calculating virial masses, we can only expect to assess the order of magnitude of the entire mass of a cloud which, in our case, confirms the necessity of a large amount of additional mass such as ionised gas or dark matter to stabilise the HVCs observed in our survey.

5.2. The origin of the HVCs

One possible origin of the HVCs observed around M 31 and M 33 could be tidal stripping of gas during close encounters with dwarf galaxies. Thilker et al. (2004) already noticed that the complex of HVCs found south of the disk of M 31 is partly overlapping with the giant stellar stream of M 31 discovered by Ibata et al. (2001). A comparison between the optical map of the stellar stream by Ferguson et al. (2004) and our WSRT H I data (Fig. 2) shows that the HVCs are grouped along the southern edge of the stream close to the disk of M 31. This positional overlap suggests a connection between the stellar stream and the H I gas. Ferguson et al. (2004) also present the results of radial velocity measurements of the stellar component at four positions along the stream. The heliocentric radial velocities range from -550 km s^{-1} close to the disk of M 31 up to -325 km s^{-1} about 4° away from the disk. In the region of the H I gas, the radial velocities of the stellar component are in the range of about -480 km s^{-1} to -550 km s^{-1} which is partly overlapping with the velocities found for the HVCs in our survey. But, as noticed in Sect. 4.2, the velocity structure of the HVC complex is very complicated. Several filaments of clouds with different radial velocities appear to intersect each other at various angles, making a comparison with the velocities of the stellar stream challenging.

In addition to having a degree of organization into filamentary structures, it is striking that many of the H I clumps, particularly HVCs 2–6 seen in Fig. 5, have large internal velocity gradients which are typically not directed along the filaments. This circumstance suggests that even within this region of likely overall tidal origin, there may well be dynamical effects related to localised dark matter concentrations.

Another example of a cloud that is likely of tidal origin is M 31 HVC 13 which is located about half a degree south of NGC 205 and covers the same radial velocities as the gas observed towards this satellite galaxy of M 31. A possible tidal interaction between NGC 205 and M 31 was already suggested by Zwicky (1959), based on the discovery of extended, faint arms emanating from both ends of NGC 205. Recently, McConnachie et al. (2004b) reported the discovery of an arc-like feature in the distribution of blue red giant branch stars north of NGC 205 which might be part of a stellar stream originating from a tidal interaction with M 31. This presumable tidal trail, however, is located on the opposite side of NGC 205 with respect to M 31 HVC 13. Our current sensitivity has not permitted detection of a continuous H I bridge between the two objects, so a physical association remains circumstantial.

We have already noted that M 33 HVC 1 is not isolated but appears to be connected with the H I disk of M 33 by a faint gas bridge. This possible connection is suggestive of a tidal origin of M 33 HVC 1 although the potential progenitor remains unkown. The distribution of stellar sources in the INT WFC survey of M 33 (McConnachie et al. 2004a) appears to show no significant enhancement toward M 33 HVC 1 or its associated H I bridge. This suggets the progenitor of M 33 HVC 1 either: (1) is quite low in stellar mass relative to the Andromeda stream; (2) lies outside the INT survey field; or (3) has been completely integrated by M 33. It is also possible that a progenitor never existed, that is, M 33 HVC 1 never supported star formation and remains largely intact as a gaseous, primordial dark matter halo. Thus, the region around M 33 HVC 1 remains a promising target for deep optical surveys which could uncover peculiarities in the stellar distribution associated with the high-velocity H I gas.

The remaining three HVCs studied near M 31 are all isolated in position-velocity space from both the stellar stream and any known dwarf companion of M 31, making a tidal origin questionable. Another possible origin for the HVCs arises from current CDM structure formation scenarios, predicting a hierarchical formation of dark-matter haloes. Large galaxies like the Milky Way or M 31 are believed to have formed by accreting smaller dark-matter haloes and thereby growing to their current mass and size. Numerical simulations predict a large number of so-called dark-matter mini-haloes throughout the Local Group to be left over from this hierarchical process of galaxy formation (Klypin et al. 1999; Moore et al. 1999).

Recent numerical simulations by Kravtsov et al. (2004) confirmed the significant overabundance of dwarf-like dark-matter haloes in the models in comparison to the relatively small number of observed dwarf galaxies around the Milky Way. They also included a simple model of star formation in dark-matter haloes which, for the first time, can reproduce both the circular velocity function as well as the radial distribution of dwarf galaxies around the Milky Way. For the central 50 kpc around M 31 the model of Kravtsov et al. (2004) predicts only 2–5 dark-matter haloes with associated gas masses, $M_{\rm g} > 10^6\,M_\odot$, that have not undergone significant internal star formation. They concur with the conclusion of Thilker et al. (2004) that only a subset of the HVCs found near M 31 might represent primordial dark-matter haloes while the remaining clouds might be the result of tidal interaction. Our new imaging results support these conclusions. A recent complementary H I blind survey for HVCs around M 31 with the Effelsberg telescope (Westmeier et al. 2005a), however, yields no evidence for any further compact HVCs beyond the boundaries of the GBT map of Thilker et al. (2004), although extended, filamentary H I emission was found by Braun & Thilker (2004) even at larger projected distances from M 31 with the WSRT. The Effelsberg survey has a 3σ H I mass limit of about $6 \times 10^4\,M_\odot$. It reaches out to a projected distance of about 130 kpc from M 31, but it covers only a limited azimuthal range. The non-detection of additional compact H I clouds may be an indication that the thermodynamic considerations of Sternberg et al. (2002) may apply. Their calculations suggest that the H I mass associated with a particular dark mini-halo mass is a sensitive function of the ambient pressure of the circum-galactic environment. This would imply a substantial gradient of decreasing neutral gas mass with galacto-centric radius for a given dark halo mass.

6. Summary and conclusions

We have observed nine fields around M 31 and one field near M 33 in H I with the WSRT to study some of the HVCs discovered by Thilker et al. (2004) and Thilker et al. (in preparation) with arcminute resolution. In two of the nine fields around M 31 we could not detect the high-velocity gas, presumably because the emission is too diffuse and faint. In the remaining seven fields we identify about 16 individual HVCs with angular sizes of the order of $10'$, corresponding to absolute sizes of the order of 1 kpc if a distance of 780 kpc (Stanek & Garnavich 1998) is assumed for M 31. The observed H I masses are in the range of about a few times $10^4\,M_\odot$ to $6 \times 10^5\,M_\odot$. Under the assumption of gravitational stability only a very small fraction of the order of 1% of the total mass of the HVCs can be seen in neutral, atomic hydrogen, and additional mass components like ionised gas or dark matter have to be the dominant constituents. The application of the virial theorem is only of marginal suitability because it is subject to a number of restrictions which, in many cases, are not stringently fulfilled. The estimation of the dynamical masses of five of the HVCs, however, emphasises the necessity of a large fraction of undetected mass.

Twelve of the HVCs are crowded in an area of only about $1^\circ \times 1^\circ$ at a projected separation of less than 15 kpc from the disk of M 31. This remarkable complex of HVCs appears to consist of several filaments of clouds intersecting each other at various angles. Clouds along the apparent filaments have similar radial velocities. A detailed comparison suggests that the HVC complex might consist of two distinct populations of clouds which can be distinguished by their different radial velocities, velocity gradients, and mean densities. Moreover, the HVC complex is partly overlapping with the giant stellar stream of M 31 discovered by Ibata et al. (2001), suggesting a connection with the stellar stream and a tidal origin for some or most of these HVCs. The densest clumps within this region have large internal velocity gradients which are not generally associated with the orientation of nearby diffuse filaments, possibly suggesting significant local concentrations of dark mass. Another HVC near M 31 is located only half a degree south of NGC 205 and at an identical radial velocity, although the evidence for a physical association remains circumstantial. The remaining HVCs around M 31 are compact and isolated without any obvious connection with M 31 or one of its known satellite galaxies.

The HVC near M 33 is not isolated but appears to be connected with the H I disk of M 33 by a faint gas bridge. Both the HVC and the bridge share a common radial velocity gradient. This configuration is again suggestive of a late stage tidal origin, but the progenitor of the H I gas remains unknown.

The modest number of isolated HVC detections seem to be in agreement with the numerical simulations of Kravtsov et al. (2004) which predict only 2–5 primordial dark-matter mini-haloes within the field of the GBT survey by Thilker et al. (2004). However, a complementary H I survey of M 31 with the Effelsberg telescope by Westmeier et al. (2005a), reaching out to a projected distance of about 130 kpc from M 31, reveals no further compact HVCs beyond the boundaries of the GBT map down to an H I mass limit of about $6 \times 10^4\,M_\odot$. The concentration of H I detections at relatively small galacto-centric radii may be consistent with the calculations of Sternberg et al. (2002) which suggest a rapidly declining neutral fraction associated with a given dark halo mass for a decreasing ambient pressure in a circum-galactic environment.

Acknowledgements. T.W. acknowledges support by the Deutsche Forschungsgemeinschaft (German Research Foundation) through project number KE757/4–1. The Westerbork Synthesis Radio Telescope is operated by the ASTRON (Netherlands Foundation for Research in Astronomy) with support from the Netherlands Foundation for Scientific Research (NWO).

References

Banks, T., Dodd, R. J., & Sullivan, D. J. 1995, MNRAS, 272, 821
Blitz, L., Spergel, D. N., Teuben, P. J., Hartman, D., & Burton, W. B. 1999, ApJ, 514, 818
Braun, R. 1997, ApJ, 484, 637
Braun, R., & Burton, W. B. 1999, A&A, 341, 437
Braun, R., & Burton, W. B. 2001, A&A, 375, 219
Braun, R., & Thilker, D. A. 2004, A&A, 417, 421
Brüns, C., Kerp, J., Kalberla, P. M. W., & Mebold, U. 2000, A&A, 357, 120
Brüns, C., Kerp, J., & Pagels, A. 2001, A&A, 370, L26

McConnachie, A. W., Ferguson, A., Huxor, A., et al. 2004a, INT Newsletter, 8, 8
McConnachie, A. W., Irwin, M. J., Lewis, G. F., et al. 2004b, MNRAS, 351, L94
Davies, R. D. 1975, MNRAS, 170, 45P
Ferguson, A. M. N., Chapman, S., Ibata, R., et al. 2004, in the proceedings of the ESO Workshop Planetary Nebulae beyond the Milky Way, ed. J. Walsh, & L. Stanghellini, in press
Gardiner, L. T., & Noguchi, M. 1996, MNRAS, 278, 191
Hartmann, D., & Burton W. B. 1997, Atlas of Galactic Neutral Hydrogen (Cambridge University Press)
de Heij, V., Braun, R., & Burton, W. B. 2002, A&A, 391, 67
Huchtmeier, W. K. 1978, IAUS, 77, 197
Ibata, R., Irwin, M., Lewis, G., Ferguson, A. M. N., & Tanvir, N. 2001, Nature, 412, 49
Klypin, A., Kravtsov, A. V., Valenzuela, O., & Prada, F. 1999, ApJ, 522, 82
Kravtsov, A. V., Gnedin, O. Y., & Klypin, A. A. 2004, ApJ, 609, 482
Lee, M. G., Kim, M., Sarajedini, A., Geisler, D., & Gieren, W. 2002, ApJ, 565, 959
Mathewson, D. S., Cleary, M. N., & Murray, J. D. 1974, ApJ, 190, 291
Moore, B., Ghigna, S., Governato, G., et al. 1999, ApJ, 524, L19
Muller, C. A., Oort, J. H., & Raimond, E. 1963, C. R. Acad. Sci. Paris, 257, 1661
Oort, J. H. 1966, Bull. Astr. Inst. Netherlands, 18, 421
Pisano, D. J., Barnes, D. G., Gibson, B. K., et al. 2004, ApJ, 610, L17
Putman, M. E., Gibson, B. K., Staveley-Smith, L., et al. 1998, Nature, 394, 752
Putman, M. E., Bland-Hawthorn, J., Veilleux, S., et al. 2003, ApJ, 597, 948
Rasmussen, A., Kahn, S. M., & Paerels, F. 2003, in The IGM/Galaxy Connection: The Distribution of Baryons at $z = 0$, ed. J. L. Rosenberg, & M. E. Putman, ASSL Conf. Proc., 281, 109
Sembach, K. R., Wakker, B. P., Savage, B. D., et al. 2003, ApJS, 146, 165
Shapiro, P. R., & Field, G. B. 1976, ApJ, 205, 762
Stanek, K. Z., & Garnavich, P. M. 1998, ApJ, 503, L131
Sternberg, A., McKee, C. F., & Wolfire, M. G. 2002, ApJS, 143, 419
Thilker, D. A., Braun, R., Walterbos, R. A. M., et al. 2004, ApJ, 601, L39
Tufte, S. L., Wilson, J. D., Madsen, G. J., Haffner, L. M., & Reynolds, R. J. 2002, ApJ, 572, L153
Wakker, B. P., & van Woerden, H. 1997, ARA&A, 35, 217
Westmeier, T., Brüns, C., & Kerp, J. 2005a, in Extraplanar Gas, ed. R. Braun, ASP Conf. Ser., 331, 105
Westmeier, T., Brüns, C., & Kerp, J. 2005b, A&A, 432, 937
Zwaan, M. 2001, MNRAS, 325, 1142
Zwicky, F. 1959, Handbuch der Physik, 53, ed. S. Flügge (Berlin: Springer-Verlag)